RSC Advances

ROYAL SOCIETY OF CHEMISTRY

www.rsc.org/advances

Cite this: DOI: 10.1039/c0xx00000x

www.rsc.org/xxxxxx

ARTICLE TYPE

Construction of g-C_3N_4/S-g-C_3N_4 metal-free isotype heterojunctions with the enhanced charge driving force and their photocatalytic performance under anoxic condition

Shaozheng Hu [a], Lin Ma [a], Fayun Li [a], Zhiping Fan [a], Qiong Wang [a], Jin Bai [a], Xiaoxue Kang [a] and Guang Wu [b,*]

Received (in XXX, XXX) Xth XXXXXXXXX 20XX, Accepted Xth XXXXXXXXX 20XX
DOI: 10.1039/b000000x

In the heterojunctions catalysts, the potential difference is the main driving force for efficient charge separation and transfer. The slight difference in the electronic band structure of the isotype heterojunctions catalysts causes the poor driving force, leading to the dissatisfactory charge separation efficiency. In this work, g-C_3N_4/S-g-C_3N_4 metal-free isotype heterojunctions catalysts (GCN-SCN) with the enhanced charge driving force were prepared by a two step calcination method. Anoxic photocatalytic degradation of RhB under visible light was used to evaluate the performance of as-prepared g-C_3N_4 catalysts. The results indicate that this two step calcination method can markedly promote the charge driving force of as-prepared isotype heterojunctions, leading to the more efficient charge-carrier migration. GCN-SCN displays the highest reaction rate constant of 0.0228 min^{-1}, which is 3.5 and 2.9 times higher than that of GCN/SCN(1) and GCN/SCN(2), prepared by one step calcination method. The linear relationship is observed between VB driving force and RhB degradation rate. This paper provides a new perspective to prepare the isotype heterojunctions with promoted charge driving force and photocatalytic performance.

Introduction

As a clean and green technology, photocatalytic oxidation technology has received more and more attentions. In general, a photocatalysis process requires the participation of molecular oxygen, which can generate reactive oxygen species by capturing electrons. However, oxygen is not available in many environments, such as petroleum-contaminated aquifers, oil reservoirs and deep sediments.[1] These anoxic environments would suppress the ability of traditional photocatalysts. Therefore, the design and synthesis of novel photocatalysts for the anoxic photocatalytic process is required. In recent years, graphitic carbon nitride (g-C_3N_4), the most stable allotrope of covalent carbon nitride, have been widely used as a new metal-free visible light photocatalyst for organic pollutant degradation,[2] water reduction and oxidation,[3] CO_2 capture[4] and organic synthesis.[5] The tunable condensation degree and distinctive heptazine ring structure make g-C_3N_4 possess good physicochemical stability, fascinating electronic structure and medium band gap (2.7 eV).[6,7] These advantages make g-C_3N_4 become a potential candidate for visible light photocatalyst. Besides that, g-C_3N_4 is composed of very common elements, C, N and H. It is easily prepared via one-step polymerization of cheap raw materials, such as melamine,[8] dicyandiamide,[9] urea[10] and thiourea.[11] Nevertheless, the shortcomings of g-C_3N_4 are as obvious as its advantages, such as the low visible light utilization efficiency and rapid recombination of photogenerated electron-hole. To advance this promising photocatalyst, many strategies have been used, such as metal and non-metal doping,[12-15] copolymerization,[16] semiconductor coupling[17] and nanostructured design.[18]

The semiconductor coupling is one of the most promising method among which mentioned above. In the photocatalysis field, the construction of intimate heterojunction between two appropriate semiconductors is an effective strategy to enhance the photocatalytic performance. Several kinds of g-C_3N_4-based heterojunctions have been developed by coupling g-C_3N_4 with other types of inorganic photocatalysts, such as graphene/g-C_3N_4,[19] TiO_2/g-C_3N_4,[20] MoS_2/g-C_3N_4,[21] CdS/g-C_3N_4[22] and WO_3/g-C_3N_4.[23] However, a basic condition has to be satisfied to form the heterojunction: the energy level matching of two semiconductors. This condition limits the further development of this method.

Recently, inspired by Degussa P25 (a mixture of 75% anatase-TiO_2 and 25% rutile-TiO_2), constructing isotype heterojunctions between two different crystal phases of a single substance has been developed.[24-26] The slight difference in the electronic band structure between two different crystal phases of a single substance enables the formation of isotype junction at their crystal interfaces. In general, the band gap structure of g-C_3N_4 can be simply tuned from 2.4 to 2.8 eV by using different precursors, coupling two components of g-C_3N_4 with well-matched band structure forming a g-C_3N_4/g-C_3N_4 isotype

heterojunction can provide an alternative novel pathway to address the intrinsic drawbacks of g-C_3N_4 to enhance the photocatalytic performance without relying on extra semiconductors. Zhang et al. prepared g-C_3N_4/S-doped g-C_3N_4 heterojunction photocatalyst using trithiocyanuric acid and dicyandiamide as raw materials.[24] The obtained heterojunction was demonstrated to promote charge separation which arises from the band offsets, leading to a significant enhancement in the photocatalytic hydrogen production. Dong et al. prepared g-C_3N_4/g-C_3N_4 isotype heterojunction using urea and thiourea as raw materials.[25,26] They suggested that the lifetime of charge carriers was prolonged driven by the band offsets in this isotype heterojunction catalyst, resulting in the improved photocatalytic NO removal ability under visible light irradiation.

All of these reported g-C_3N_4 based isotype heterojunctions are prepared using different precursors. However, the potential difference between the two components of heterojunctions is the main driving force for efficient charge separation and transfer.[24,27,28] The slight difference in the electronic band structure of these isotype heterojunctions catalysts causes the poor driving force, leading to the dissatisfactory charge separation efficiency. It is known that the calcination temperature is the key factor to determine the polycondensation degree. Besides that, polycondensation degree of different precursor at the same calcination temperature is also different, thus leading to the different band structure. Therefore, compared with one-step calcination method, the two-step calcination method (520 ^oC for 2 h at a rate of 5 $^oC \cdot min^{-1}$ and then 550 ^oC for 4 h at a rate of 10 $^oC \cdot min^{-1}$) can make different precursor exhibit the polycondensation degree in greater difference, which can promote the charge driving force and improve the photocatalytic performance. Here, we report a g-C_3N_4/S-g-C_3N_4 metal-free isotype heterojunctions catalyst with the enhanced charge driving force prepared by a two step calcination method. The charge driving force can be promoted more than two times by this two step calcination method, leading to the more efficient charge-carrier migration. Anoxic photocatalytic degradation of RhB under visible light was used to evaluate the performance of as-prepared g-C_3N_4 catalysts.

Experimental

Preparation and characterization

All chemicals used in this study were analytical grade and without further treatment. 6 g of urea or thiourea was calcined at 520 ^oC for 2 h (at a rate of 5 $^oC \cdot min^{-1}$). The prepared catalyst is referred to as GCN(1) or SCN(1). 6 g of urea or thiourea was calcined at 550 ^oC for 4 h (at a rate of 10 $^oC \cdot min^{-1}$). The prepared catalyst is referred to as GCN(2) or SCN(2). 6 g of thiourea was dissolved into 20 mL deionized water to form the solution. 1 g of as-prepared GCN(1) was added into the above solution and ultrasound-treated for additional 60 min. After that, the mixture was stirred vigorously for another 2 h to achieve homogeneous suspension. The obtained suspension was heated to 100 ^oC to remove the water. The solid product was dried at 100 ^oC in oven, followed by milling and annealing at 550 ^oC for 4 h (at a rate of 10 $^oC \cdot min^{-1}$). The obtained product was GCN-SCN. Neat SCN was prepared by two-step annealing thiourea: 520 ^oC for 2 h (at a rate of 5 $^oC \cdot min^{-1}$) and then 550 ^oC for 4 h (at a rate of 10 $^oC \cdot min^{-1}$). For comparison, GCN was prepared following the same procedure as in the synthesis of GCN-SCN but in the absence of thiourea.

In order to confirm the effect of this two step calcination method on the promotion of charge driving force, g-C_3N_4/S-g-C_3N_4 isotype heterojunctions were prepared by one step calcination method. 6 g of thiourea and 6 g of urea were dissolved into 30 mL water. The solution was then dried at 100 °C to remove the water and get the molecular composite precursors. The precursors were calcined by two different methods, 520 °C for 2 h at a heating rate of 5 $^oC \cdot min^{-1}$ and 550 °C for 4 h at a heating rate of 10 $^oC \cdot min^{-1}$. The resultant products were denoted as GCN/SCN(1) and GCN/SCN(2), respectively.

The XRD patterns of the prepared samples were recorded on a Rigaku D/max-2400 instrument using Cu-Kα radiation (λ = 1.54 Å). The scan rate, step size, voltage and current were 0.05 ^{o}/min, 0.01 ^{o}, 40 kV and 30 mA, respectively. Elemental analysis was performed with a vario EL cube from Elementar Analysensysteme GmbH. UV-Vis spectroscopy was carried out on a JASCO V-550 model UV-Vis spectrophotometer using $BaSO_4$ as the reflectance sample. The XPS measurements were performed on a Thermo Escalab 250 XPS system with Al Kα radiation as the excitation source. The binding energies were calibrated by referencing the C 1s peak (284.6 eV) to reduce the sample charge effect. Nitrogen adsorption was measured at -196 °C on a Micromeritics 2010 analyser. All the samples were degassed at 393 K prior to the measurement. The BET surface area (S_{BET}) was calculated based on the adsorption isotherm. The photoluminescence (PL) spectra were measured at room temperature with a fluorospectrophotometer (FP-6300) using a Xe lamp as the excitation source. The electrochemical impedance spectra (EIS) were recorded using an EIS spectrometer (EC-Lab SP-150, BioLogic Science Instruments) in a three electrode cell by applying a 10 mV alternative signal versus the reference electrode (SCE) over a frequency range of 1 MHz to 100 mHz. The cyclic voltammograms were measured in a 0.1 M KCl solution containing 2.5 mM $K_3[Fe(CN)_6]/K_4[Fe(CN)_6]$ (1:1) as a redox probe at a scanning rate of 20 $mV \cdot s^{-1}$ in the same three electrode cell as the EIS measurement.

Photocatalytic Reaction

RhB was selected as the model compound to evaluate the anoxic photocatalytic performance of the prepared g-C_3N_4 based catalysts in an aqueous solution under visible light irradiation. A total of 0.05 g of catalyst was dispersed in 200 ml of an aqueous solution containing RhB (10 ppm) in an ultrasound generator for 10 min. The suspension was transferred to a self-designed glass reactor and stirred for 30 min in the dark to achieve adsorption equilibrium. N_2 was continuously bubbled through the solution to remove O_2 during the reaction process. In the photoreaction under visible light irradiation, the suspension was exposed to a 250 W high-pressure sodium lamp with a main emission in the 400-800 nm range, and air was bubbled at 130 ml/min through the solution. The UV light portion of the sodium lamp was filtered by a 0.5 M $NaNO_2$ solution. All the runs were conducted at ambient pressure and 30 °C. At specific time intervals, 4 ml of the suspension was removed and immediately centrifuged to separate the liquid samples from the solid catalyst. The RhB

concentrations before and after the reaction were measured using a UV-Vis spectrophotometer at a wavelength of 550 nm.

Results and discussion

Figure 1 presents the XRD patterns of as-prepared GCN, SCN and GCN-SCN. The XRD patterns confirmed the formation of graphitic carbon nitride. For GCN, the peak at 13.1° corresponds to in-plane structural packing motif of tri-s-triazine units, which is indexed as (100) peak. The distance is calculated as d = 0.675 nm, corresponding to the hole-to-hole distance in the nitride pores. The peak at 27.6 ° corresponds to interlayer stacking of aromatic segments with distance of 0.323 nm, which is indexed as (002) peak. From the Figure 1 insert, it can be seen that the diffraction angle of (002) peak for GCN (27.6 °) is higher than that of SCN (27.3 °), corresponding to the interlayer distance of GCN (0.323 nm) is shorter than that of SCN (0.326 nm). This is probably due to the additional leaving motif oxygen in urea that facilitates the condensation process and shorten the interlayer distance.[9] Further observation indicates that the diffraction angle of (002) peak for GCN-SCN (27.5 °) is located between GCN and SCN, confirming the formation of isotype heterostructure.

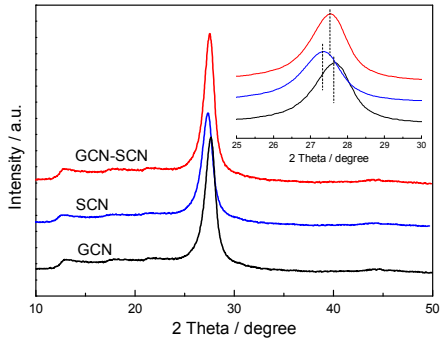

Figure 1. XRD patterns of as-prepared GCN, SCN and GCN-SCN.

Generally, a catalyst with high specific surface area (S_{BET}) and big pore volume is significant to the enhancement of catalytic performance. As present in Table 1, GCN exhibits the highest S_{BET} of 14.5 $m^2 \cdot g^{-1}$, whereas SCN and GCN-SCN have S_{BET} of 8.6 and 12.4 $m^2 \cdot g^{-1}$. This hints that the additional oxygen in the urea is beneficial for enlarging the surface area of g-C_3N_4, presumably because of the formation of CO_2 during the condensation to suppress the advance of grain boundary.[9] No essential difference in S_{BET} among three as-prepared isotype heterojunctions is observed, indicating the preparation method does not influence their S_{BET}. For the pore volume, Similar trend is shown. The C/N ratio is 0.68 for GCN, which is lower than that of SCN (0.71). This result confirms that the condensation process can be influenced by different precursors, which is consistent with XRD results. For three as-prepared isotype heterojunctions, the C/N ratio of GCN-SCN is 0.66, much smaller than that of GCN/SCN(1) and GCN/SCN(2) (0.69 and 0.70). This hints that the preparation method can influence the condensation degree of as-prepared isotype heterojunctions.

UV-Vis spectra were used to investigate the optical property and electronic band structure of the as-prepared g-C_3N_4 catalysts. As shown in Figure 2, all the samples feature an intrinsic semiconductor-like absorption. The intensity of the absorbance of SCN is higher than that of GCN in the full spectrum, accompanying with the absorption edge shift from 455 for GCN to 477 for SCN. The band gaps are estimated from the tangent lines in the plots of the square root of the Kubelka-Munk functions as a function of the photon energy (Figure 2 insert).[29] The results show that the band gap energy for GCN and SCN is 2.72 and 2.54 eV, respectively. The remarkable difference in band gap energy between GCN and SCN provide great potential for the design of g-C_3N_4 based isotype heterojunction with well-matched band structure. It is note that a broad absorption peak from 450 nm to 600 nm is observed for the SCN. Wang et al. obtained a similar result and suggested that sulfur was most likely doped into the crystal lattice of g-C_3N_4, creating more defects.[30] Wang et al. simulated the total and partial DOS of pure and S-doped g-C_3N_4 using first principle calculations and suggested that the doped S atom influenced the distribution of C and N atoms in the lattice, leading to hybrid p orbitals among the C, N and S atoms and caused a broad absorption peak at 450~600 nm. The band gap energy of GCN-SCN located between GCN and SCN (2.60 eV), which further confirmed the electronic coupling of these two components in the GCN-SCN heterojunction. In Figure S1 and S2, the band gaps for GCN(1), GCN(2), SCN(1) and SCN(2) are 2.66, 2.65, 2.55 and 2.46 eV, which are different from GCN and SCN. This confirms that the calcination method can determine the condensation degree, which significantly influences the band gap structure of g-C_3N_4. The band gap energies of GCN/SCN(1) and GCN/SCN(2) are also located between their components (2.58 and 2.57 eV, Table 1), confirming the formation of heterojunction catalysts.

Table 1 S_{BET}, pore volume, C/N ratio, band gap and rate constant of as-prepared g-C_3N_4 catalysts

Sample	S_{BET} ($m^2 \cdot g^{-1}$)	Pore volume ($cm^3 \cdot g^{-1}$)	C/N ratio	Band gap (eV)	k (min^{-1})
GCN	14.5	0.06	0.68	2.72	0.0024
SCN	8.6	0.03	0.71	2.54	0.0035
GCN-SCN	12.4	0.05	0.66	2.60	0.0228
GCN/SCN(1)	11.6	0.04	0.69	2.55	0.0064
GCN/SCN(2)	12.9	0.04	0.70	2.46	0.0080

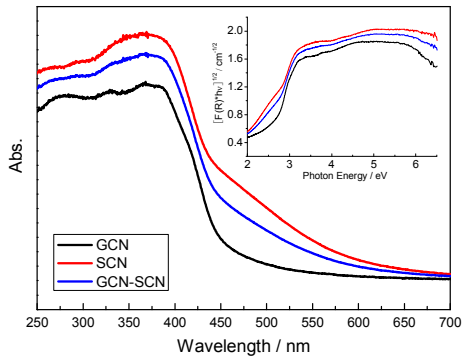

Figure 2. UV-Vis spectra of the as-prepared GCN, SCN and GCN-SCN.

To confirm the structure of g-C_3N_4 and further identify the chemical state of the sulfur element, the g-C_3N_4 based catalysts were characterized using XPS. In Figures 3a and b, the spectra of as-prepared g-C_3N_4 based catalysts in both the N 1s and C 1s regions can be fitted with two contributions. In C 1s region (Figure 3a), two components locate at 284.6 and 288 eV for GCN and SCN. The sharp peak around 284.6 eV is attributed to the pure graphitic species in the CN matrix. The peak with binding energy of 288 eV indicates the presence of sp^2 C atoms bonded to aliphatic amine ($–NH_2$ or –NH–) in the aromatic rings.[31] In Figure 3b, the main N 1s peak at a binding energy of 398.5 eV can be assigned to sp^2 hybridized nitrogen (C=N–C), thus confirming the presence of sp^2 bonded graphitic carbon nitride. The peak at higher binding energy 400.5 eV is attributed to tertiary nitrogen ($N–(C)_3$) groups.[11] The spectra of GCN-SCN in the C 1s and N 1s regions do not exhibit a shift in the binding energy. In the S 2p region (Figure 3c), no S species is found in GCN. The binding energy is located at 163.9 eV for SCN. According to the literature reported by Chen et al., this binding energy is assigned to the doping sulfur in the nitrogen position to form a S-C bond.[32] For GCN-SCN, no obvious shift in the binding energy is observed in S 2p region, suggesting that the formation of GCN-SCN heterojunction does not influence the chemical state of sulfur.

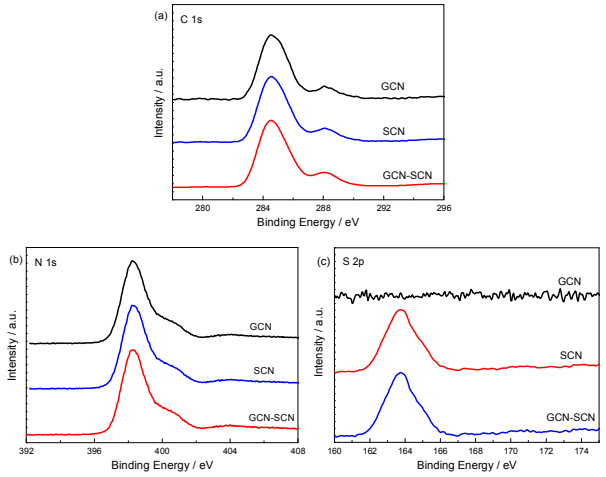

Figure 3. XPS spectra of the as-prepared g-C_3N_4 catalysts in the region of C 1s (a), N 1s (b) and S 2p (c).

The band structures of GCN and SCN were further investigated by VB XPS (Figure 4). The VB maxima of GCN and SCN are shown to be 1.52 and 1.08 eV, respectively.[27,33] The VB potential of GCN is more positive than that of SCN. Combine with the band gap energies obtained from UV-Vis spectra, the CB position of GCN and SCN are calculated to be -1.2 and -1.46 eV, indicating that the CB potential of SCN is more negative than that of GCN. On the basis of VB and CB levels of GCN and SCN, a band structure diagram for GCN-SCN isotype heterojunction can be drawn as shown in Figure 5. Once GCN and SCN are electronically coupled together, the band alignment between the two kinds of g-C_3N_4 materials results in the formation of heterojunction with well-matched band structure. Upon visible-light irradiation, the photogenerated electrons tend to transfer rapidly from SCN to GCN driven by CB offset of 0.26 eV, whereas the photogenerated holes transfer from GCN to SCN driven by VB offset of 0.44 eV. The potential difference is the main driving force for efficient charge separation and transfer. These two charge transfer processes are beneficial for overcoming the high dissociation barrier of the Frenkel exciton and stabilizing electrons and holes. The redistribution of electrons on one side of the heterojunction (GCN) and holes on the opposite side (SCN) could establish a steady internal electric fields, which reduces the electron/hole pairs recombination. As the photogenerated electrons and holes are spatially separated into two components, the charge recombination is drastically inhibited, which is of great benefit for enhancing the photocatalytic activity. In addition, with effective separation of electron/hole pairs, the lifetime of photogenerated charge carriers is expected to be prolonged. The prolonged lifetime allows the fast charge transfer to the reactive substrates on the photocatalyst surface, promoting the photocatalysis reaction.[27,28] As shown in Figure S3 and S4, the VB maxima of GCN(1), SCN(1), GCN(2) and SCN(2) are 1.54, 1.40, 1.58 and 1.38 eV, respectively. Accordingly, the CB position of GCN(1), SCN(1), GCN(2) and SCN(2) are calculated to be -1.12, -1.15, -1.07 and -1.08 eV. Thus the heterojunction catalysts GCN/SCN(1) and GCN/SCN(2) with well-matched band structure are also obtained.

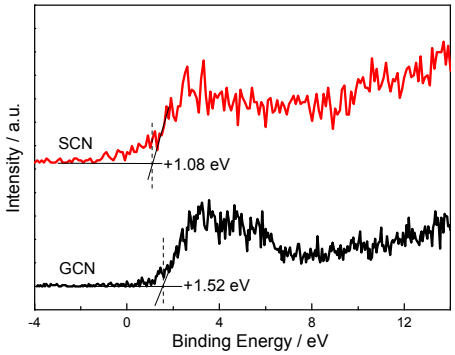

Figure 4. VB XPS of as-prepared GCN and SCN.

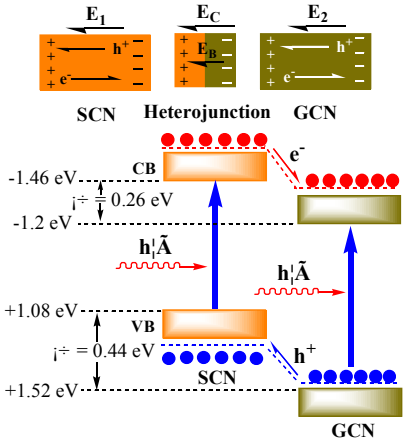

Figure 5. The schematic illustration of electron-hole separation and transport at the GCN-SCN heterojunction interface: E_C is the

contact electric field for the two components; E_B is the potential barrier in the interfacial depletion layer; E_1 and E_2 are the internal electric fields induced by the redistribution of the spatial charges in GCN and SCN, respectively.

EIS and PL spectra are very useful tools for characterizing the charge-carrier migration, and these spectra were employed to further confirm the interfacial charge transfer effect of the as-prepared g-C_3N_4 catalysts. As shown in Figure 6a, the as-prepared heterojunction catalysts exhibit decreased arc radius compared to that of GCN and SCN. In general, the radius of the arc in the EIS spectra reflects the reaction rate on the surface of the electrode.[34] The reduced arc radius indicates diminished resistance of working electrodes, suggesting a decrease in the solid state interface layer resistance and the charge transfer resistance across the solid-liquid junction on the surface between GCN and SCN.[35] GCN-SCN shows the smallest arc radius. Since the radius of the arc on the EIS spectra reflects the migration rate occurring at the surface, it suggests that a more effective separation of photogenerated electron-hole pairs and a faster interfacial charge transfer occurs on GCN-SCN surface.[36] In general, at a lower PL intensity, the separation rate of the photogenerated electron-hole pairs is higher. In Figure 6b, the PL intensity follows the sequence: GCN-SCN < GCN/SCN(2) < GCN/SCN(1) < SCN < GCN. This order in the degree of PL quenching is consistent with the arc radius shown in the EIS spectra, confirming the efficient transfer of photoinduced electrons and holes in GCN-SCN.

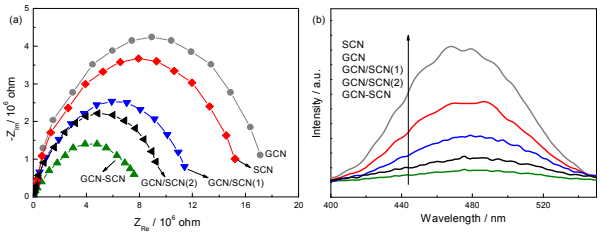

Figure 6. EIS and PL spectra of the as-prepared g-C_3N_4 catalysts.

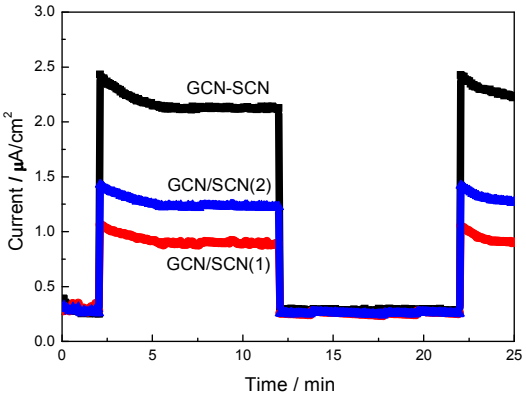

Figure 7. The photocurrent responses of as-prepared metal-free isotype heterojunctions catalysts.

The I-t curve is provided to compare the carrier separation ability of as-prepared heterojunction catalysts (Figure 7). The decay of the photocurrent indicates that partial h^+ which arrived the catalyst surface does not capture e^- from the electrolyte but accumulates at the surface or recombined with electrons from the conduction band. After the recombination of the excessive h^+, the generation and transfer of electron-hole pairs reach equilibration, and a stable photocurrent is formed. The photocurrent value of GCN-SCN is obviously higher than that of GCN/SCN(1) and GCN/SCN(2), which can be attributed to the more efficient separation of photogenerated electron-hole pairs. This is consistent with the PL and EIS results.

Figure 8. Anoxic photocatalytic degradation performance of RhB

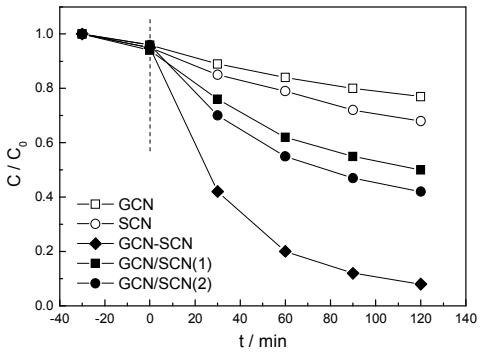

over the as-prepared g-C_3N_4 catalysts under visible light.

The anoxic photocatalytic performance of the as-prepared catalysts was evaluated by studying the degradation of RhB, which has positively charged organic end groups, in the absence of oxygen (Figure 8). The pH of the RhB solutions is 6.1 during the anoxic photodegradation process. Due to the high recombination rate of the electrons and holes, GCN and SCN show the low degradation rates (~23% and 32%) and reaction rate constants (0.0024 and 0.0035 min^{-1}), as shown in Table 1. For GCN/SCN(1) and GCN/SCN(2), the activities (reaction rate constants) increase to 50% (0.0064 min^{-1}) and 58% (0.008 min^{-1}). GCN-SCN displays the highest anoxic photocatalytic performance, 92% and 0.0228 min^{-1}, which is 3.5 and 2.9 times higher than that of GCN/SCN(1) and GCN/SCN(2). The RhB photocatalytic degradation performance of as-prepared heterojunction catalysts were compared in the presence of oxygen (Figure S5). It is shown that the presence of oxygen does not remarkably promote the activity over as-prepared heterojunction catalysts, indicating that molecular oxygen is not necessary for the photocatalytic oxidation of RhB in current system.

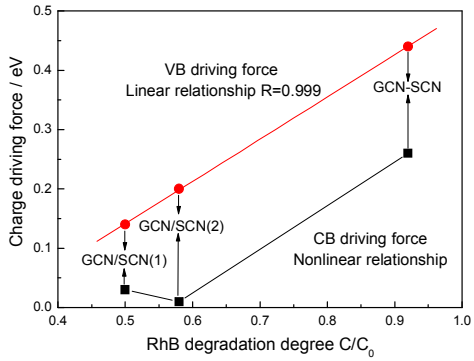

Figure 9. The relationship between charge driving force and RhB degradation degree of as-prepared metal-free isotype heterojunctions catalysts.

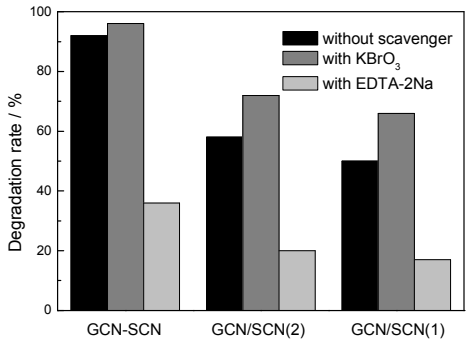

Figure 10. The influence of various scavengers on the visible light photocatalytic activity of as-prepared heterojunction catalysts.

From the UV-Vis and VB XPS results, it is calculated that the VB driving force for GCN-SCN, GCN/SCN(1) and GCN/SCN(2) is 0.44, 0.14 and 0.2 eV, respectively. Accordingly, the CB driving force for GCN-SCN, GCN/SCN(1) and GCN/SCN(2) is 0.26, 0.03 and 0.01 eV, respectively. Figure 9 shows the relationship between charge driving force and RhB degradation rate of as-prepared metal-free isotype heterojunctions catalysts. Interestingly, the linear relationship is observed between VB driving force and RhB degradation rate. The larger VB driving force, the higher RhB degradation rate. GCN-SCN with the enhanced charge driving force shows much higher RhB degradation rate than that of GCN/SCN(1) and GCN/SCN(2). Nonlinear relationship is shown in Figure 9 between CB driving force and RhB degradation rate. It is known that VB and CB driving forces determine the migration rate of photogenerated holes and electrons, respectively. This indicates that photogenerated holes are responsible for the photocatalytic oxidation of RhB in current system. This is consistent with the reaction results. In the photocatalytic process, photogenerated electrons can trap the molecular oxygen to form the reactive oxygen species.[37] The reaction results indicate that molecular oxygen is not necessary for the photocatalytic oxidation of RhB in current system. Thus it is reasonable that the nonlinear relationship is observed between CB driving force and RhB degradation rate. In summary, the linear relationship is observed between VB driving force and RhB degradation rate. GCN-SCN with the enhanced charge driving force prepared by a two step calcination method shows much higher RhB degradation rate than that of GCN/SCN(1) and GCN/SCN(2). This paper provides a new perspective to prepare the isotype heterojunctions with promoted charge driving force and photocatalytic performance.

In order to determine of the role of electrons and holes in photodegradation process, EDTA-2Na and $KBrO_3$ are used as the hole (h^+) and electron (e^-) scavenger, respectively.[38-40] Figure 10 shows the influence of various scavengers on the visible light photocatalytic activity of as-prepared heterojunction catalysts. With the addition of EDTA-2Na, the RhB degradation rate for GCN-SCN, GCN/SCN(2), and GCN/SCN(1) decreased from 92%, 58% and 50% to 36%, 20% and 17%, respectively. This indicates that photogenerated holes are the main active species for RhB degradation. When $KBrO_3$ was added, the RhB degradation rate for GCN-SCN, GCN/SCN(2) and GCN/SCN(1) did not decrease but increased to 96%, 72% and 66%, respectively. This is probably due to that the addition of $KBrO_3$ to trap the electrons can promote the separation rate of e^-/h^+ pairs, leading to the increased photocatalytic performance.

Conclusions

GCN-SCN, g-C_3N_4/S-g-C_3N_4 metal-free isotype heterojunctions catalyst, was prepared by a two step calcination method. Compared with the isotype heterojunctions catalysts prepared by one step calcination method, GCN/SCN(1) and GCN/SCN(2), the charge driving force of GCN-SCN is promoted more than two times, leading to the more efficient charge-carrier migration. The results of RhB anoxic photocatalytic degradation indicate that, GCN-SCN displays the highest reaction rate constant of 0.0228 min^{-1}, which is 3.5 and 2.9 times higher than that of GCN/SCN(1) and GCN/SCN(2). The molecular oxygen is not necessary but photogenerated holes are responsible for the photocatalytic oxidation of RhB in current system. The linear relationship is observed between VB driving force and RhB degradation rate. This paper provides a new perspective to prepare the isotype heterojunctions with promoted charge driving force and photocatalytic performance.

Acknowledgment

This work was supported by Science & Technology Research Foundation of Heilongjiang Province Education Bureau of China (No.12541626), Postdoctoral Fund of Heilongjiang province of China (No. LBH-Z14208), Education Department of Liaoning Province (No. L2014145), Environmental Science and Engineering Innovation Team of Liaoning Shihua University ([2014]-11), and Students' Innovation Fund Project of China.

Notes and references

[a] *College of Chemistry, Chemical Engineering, and Environmental Engineering, Liaoning Shihua University, Fushun 113001, China*
[b] *School of Chemistry and Materials Sciences, Heilongjiang University; Key Laboratory of Chemical Engineering Processes & Technology for High-efficiency Conversion (College of Heilongjiang Province), Harbin 150080, China. E-mail: guangw001@163.com*

1 C.C. Chen, W.H. Ma and J.C. Zhao, *Chem. Soc. Rev.,* 2010, **39**, 4206.
2 S.Z. Hu, F.Y. Li, Z.P. Fan, F. Wang, Y.F. Zhao and Z.B. Lv, *Dalton Trans.,* 2015, **44**, 1084.
3 X.C. Wang, K. Maeda, A. Thomas, K. Takanabe, G. Xin, J.M. Carlsson, K. Domen and M. Antonietti, *Nat. Mater.,* 2009, **8**, 76.
4 Q.F. Deng, L. Liu, X.Z. Lin, G.H. Du, Y.P. Liu and Z.Y. Yuan, *Chem. Eng. J.,* 2012, **203**, 63.
5 M.B. Ansari, H.L. Jin, M.N. Parvin and S.E. Park, *Catal. Today,* 2012, **185**, 211.
6 G. Liu, L.Z. Wang, H.G. Yang, H.M. Cheng and G.Q. Lu, *J. Mater. Chem.,* 2010, **20**, 831.
7 D.Q. Zhang, G.S. Li and J.C. Yu, *J. Mater. Chem.,* 2010, **20**, 4529.
8 Y.J. Wang, Z.X. Wang, S. Muhammad and J. He, *CrystEngComm,* 2012, **14**, 5065.
9 G.G. Zhang, J.S. Zhang, M.W. Zhang and X.C. Wang, *J. Mater. Chem.,* 2012, **22**, 8083.
10 F. Dong, L.W. Wu, Y.J. Sun, M. Fu, Z.B. Wu and S.C. Lee, *J. Mater. Chem.,* 2011, **21**, 15171.
11 Y.W. Zhang, J.H. Liu, G. Wu and W. Chen, *Nanoscale,* 2012, **4**, 5300.
12 Y.J. Zhang, T. Mori, J.H. Ye and M. Antonietti, *J. Am. Chem. Soc.,* 2010, **132**, 6294.
13 Y.Y. Bu, Z.Y. Chen and W.B. Li, *Appl. Catal. B: Environ.,* 2014, **144**, 622.
14 C. Chang, Y. Fu, M. Hu, C.Y. Wang, G.Q. Shan and L.Y. Zhu, *Appl. Catal. B: Environ.,* 2013, **142-143**, 553.
15 J.D. Hong, X.Y. Xia, Y.S. Wang and R. Xu, *J. Mater. Chem.,* 2012, **22**, 15006.
16 J.S. Zhang, X.F. Chen, K. Takanabe, K. Maeda, K. Domen, J.D. Epping, X.Z. Fu, M. Antonietti and X.C. Wang, *Angew. Chem. Int. Ed.,* 2010, **49**, 441.
17 C.S. Pan, J. Xu, Y.J. Wang, D. Li and Y.F. Zhu, *Adv. Funct. Mater.,* 2012, **22**, 1518.
18 X.C.Wang, K. Maeda, X.F. Chen, K. Takanabe and K. Domen, *J. Am. Chem. Soc.,* 2009, **131**, 1680.
19 G.Z. Liao, S. Chen, X. Quan, H.T. Yu and H.M. Zhao, *J. Mater. Chem.,* 2012, **22**, 2721.
20 K. Sridharan, E. Jang and T.J. Park, *Appl. Catal. B: Environ.,* 2013, **142-143**, 718.
21 L. Ge, C.C. Han, X.L. Xiao and L.L. Guo, *Inter. J. Hydrogen Energy,* 2013, **38**, 6960.
22 M.L. Lu, Z.X. Pei, S.X. Weng, W.H. Feng, Z.B. Fang, Z.Y. Zheng, M.L. Huang and P. Liu, *Phys. Chem. Chem. Phys.,* 2014, **16**, 21280.
23 M. Yang, S.Z. Hu, F.Y. Li, Z.P. Fan, F. Wang, D. Liu and J.Z. Gui, *Ceram. Inter.,* 2014, **40**, 11963.
24 J.S. Zhang, M.W. Zhang, R.Q. Sun and X.C. Wang, *Angew. Chem. Int. Ed.,* 2012, **51**, 10145.
25 F. Dong, Z.W. Zhao, T.Xiong, Z.L. Ni, W.D. Zhang, Y.J. Sun and W.K. Ho, *ACS Appl. Mater. Inter.,* 2013, **5**, 11392.
26 F. Dong, Z.L. Ni, P.D. Li and Z.B. Wu, *New J. Chem.,* 2015, **39**, 4737.
27 X. Wang, Q. Xu, M. Li, S. Shen, X. Wang, Y. Wang, Z. Feng, J. Shi, H. Han and C. Li, *Angew. Chem. Int. Ed.,* 2012, **51**, 13089.
28 J. Hou, C. Yang, Z. Wang, W. Zhou, S. Jiao and H. Zhu, *Appl. Catal. B: Environ.,* 2013, **142-143**, 504.
29 Y.I. Kim, S.J. Atherton, E.S. Brigham and T.E. Mallouk, *J. Phys. Chem.* 1993, **97**, 11802.
30 K. Wang, Q. Li, B. Liu, B. Cheng, W. Ho and J.G. Yu, *Appl. Catal. B: Environ.,* 2015, **176**, 44.
31 W. Lei, D. Portehault, R. Dimova and M. Antoniettit, *J. Am. Chem. Soc.,* 2011, **133**, 7121.
32 G. Liu, P. Niu, C.H. Sun, S.C. Smith, Z.G. Chen, G.Q. Lu and H.M. Cheng, *J. Am. Chem. Soc.,* 2010, **132**, 11642.
33 S. Chu, Y. Wang, Y. Guo, J. Feng, C. Wang, W. Luo, X. Fan and Z.G. Zou, *ACS Catal.,* 2013, **3**, 912.
34 Y. Xu, H. Xu, L. Wang, J. Yan, H. Li, Y. Song, L. Huang and G. Cai, *Dalton Trans.,* 2013, **42**, 7604.
35 B.L. He, B. Dong and H.L. Li, *Electrochem. Commun.,* 2007, **9**, 425.
36 Q.W. Huang, S.Q. Tian, D.W. Zeng, X.X. Wang, W.L. Song, Y.Y. Li, W. Xiao and C.S. Xie, *ACS Catal.,* 2013, **3**, 1477.
37 M.R. Hoffmann, S.T. Martin, W. Choi and D.W. Bahnemann, *Chem. Rev.,* 1995, **95**, 69.
38 S.Q. Zhang, Y.X. Yang, Y.N. Guo, W. Guo, M. Wang,Y.H. Guo and M.X. Huo, *J. Hazard. Mater.,* 2013, **261**, 235.
39 M. Muneera and D. Bahnemannb, *Appl. Catal. B: Environ.,* **2002**, *36*, 95.
40 W. Liu, S.F. Chen, W. Zhao and S.J. Zhang, *J. Hazard. Mater.,* **2009**, *164*, 154